J Biomed Mater Res Part A 2013:101A:1248–1254. (Accepted Version)

Improving the packing density of calcium phosphate coating on a magnesium alloy for enhanced degradation resistance

M. Bobby Kannan *

Discipline of Chemical Engineering, School of Engineering and Physical Sciences, James Cook University, Townsville, Queensland 4811, Australia

Abstract

In this study, an attempt was made to improve the packing density of calcium phosphate (CaP) coating on a magnesium alloy by tailoring the coating solution for enhanced degradation resistance of the alloy for implant applications. An organic solvent, ethanol, was added to the coating solution to decrease the conductivity of the coating solution so that hydrogen bubble formation/bursting reduces during the CaP coating process. Experimental results confirmed that ethanol addition to the coating solution reduces the conductivity of the solution and also decreases the hydrogen evolution/bubble bursting. In vitro electrochemical experiments i.e. electrochemical impedance spectroscopy (EIS) and potentiodynamic polarization showed that CaP coating produced in 30 % (v/v) ethanol containing coating solution (3E) exhibits significantly higher degradation resistance (i.e., ~50% higher polarisation resistance and ~60% lower corrosion current) than the aqueous solution coating. Scanning electron microscope (SEM) analysis of the coatings revealed that the packing of 3E coating was denser than that of aqueous coating, which can be attributed to the lower hydrogen evolution in the former than in the latter. Further increase in the ethanol content in the coating solution was not beneficial; in fact the coating produced in 70% (v/v) ethanol

* Corresponding author. Tel.: +61 7 4781 5080; fax: +61 7 4781 6788; e-mail: bobby.mathan@jcu.edu.au

containing solution (7E) showed degradation resistance much inferior to that of the aqueous coating, which is due to low thickness of 7E coating.

Key words: magnesium; calcium phosphate; degradation; electrochemistry

INTRODUCTION

In recent years, magnesium and its alloys have been researched extensively for biodegradable implant applications.[1-5] However, the extremely high degradation rate of magnesium in body fluid is a major issue.[1,2] Alloying has only improved the degradation resistance of magnesium to a small degree,[3-6] due to the poor passivation behaviour of magnesium in chloride-containing environment.[7]

Calcium phosphates (CaP) have been widely researched for implant applications because of their analogy to the inorganic component of natural bones.[8] Implant materials such as stainless steels and titanium alloys have been coated with CaP for their high biocompatibility and good bio-affinity.[9-11] The osteoconductivity of CaP and the slow replacement by the host bone after implantation [12,13] make them very attractive for coating on magnesium and its alloys. A number of high temperature coating methods e.g. plasma-spraying and sputtering processes,[14] are available for CaP coating on metallic substrates, but the decomposition of the coating material at high temperature can be an issue. Electrochemical coating methods are more attractive for this purpose because these methods are generally operated at room temperature and can practically coat complex structures such as screw implants. Recently, two electrochemical methods i.e. galvanostatic (constant-current) and potentiostatic (constant-potential), have been used for coating CaP on magnesium alloys.[15-17] Generally, these conventional electrochemical methods create imperfections in the coating due to hydrogen evolution,

which is a predominant cathodic reaction for magnesium and its alloys, during the coating process. The hydrogen gas bubbles can adhere to the metal and inhibit nucleation and deposition of the coating material and lead to non-uniform coating. In addition, hydrogen bubbles bursting could also damage the already formed coating. Hence, there is potential to further improve the coating performance i.e. by reducing hydrogen evolution during the coating process.

Potentiostatic method is a better method for coating CaP on magnesium and its alloys than galvanostatic method because in the latter method the electrochemical potential decreases with time and as a consequence the hydrogen evolution also increases. The electrochemical mechanism of CaP formation is given in the below equations 1-4:[18]

$$H_2PO_4^- \longrightarrow HPO_4 + H^+ \quad (1)$$

$$2H_2O + 2e^- \longrightarrow H_2 + 2OH^- \quad (2)$$

$$OH^- + H_2PO_4^- \longrightarrow H_2O + HPO_4^{2-} \quad (3)$$

$$Ca^{2+} + HPO_4^{2-} + 2H_2O \longrightarrow CaHPO_4.2H_2O \quad (4)$$

It can be seen from the above equations that hydrogen evolution reaction is an essential reaction for precipitation of CaP. However, increase in the hydrogen evolution reaction will form large hydrogen bubbles on the metal surface which obviously affect the coating process. Hence, it is critical to control the hydrogen evolution during the coating process to form a uniform coating on the metal substrate. The hypothesis made here is that by decreasing the conductivity of the coating solution the hydrogen evolution can be controlled. The decrease in the conductivity of the coating solution

would obviously slow down the coating process but more importantly it could reduce hydrogen bubble formation.

In this study, an organic solvent, ethanol, was added to the coating solution to decrease hydrogen evolution during the coating process to produce a highly dense CaP coating for improved degradation resistance.

MATERIALS AND METHODS

A magnesium alloy, AZ91, was used as the base material in this study. The chemical composition of the alloy is given in Table I. Electrochemical coating of CaP on AZ91 magnesium alloy was carried out using constant-potential method. A typical three electrode system i.e. the sample as the working electrode, graphite as the counter electrode and Ag/AgCl as the reference electrode, was used for coating purpose. CaP was coated on flat samples (3.5 × 2 × 0.5 cm). Prior to coating, the samples were ground with SiC papers up to 2500 grit and then polished using alumina powder paste (6 μm), followed by ultrasonic cleaning in acetone and then in ethanol. The coating solution was 0.1 M $Ca(NO_3)_2$ and 0.06 M of $NH_4H_2PO_4$, the coating produced from this solution is hereafter mentioned as aqueous coating. An organic solvent, ethanol, was added to the coating solution in different proportions i.e.10%, 30%, 50% and 70% (v/v), and the coatings produced from these solutions are hereafter mentioned as 1E, 3E, 5E and 7E, respectively. The CaP coating was performed at a constant-potential of -3 $V_{Ag/AgCl}$ (based on previous study)[17] for 30 mins. The conductivity of the coating solutions was measured using a conductivity meter (EcoSense EC300). The surface morphology of the coating was examined using scanning electron microscope (SEM). The coating thickness was measured using Dual Scope® coating thickness gauge. The chemical

structure and composition of coatings were analyzed using Fourier Transform Infrared (FTIR) Spectroscopy (PerkinElmer) and X-ray diffraction (XRD).

In vitro degradation tests were carried out in simulated body fluid (SBF) maintained at a physiological pH value of 7.4 and temperature of 37±0.5^{o}C. The chemical composition of the SBF is shown in Table II.[19] The SBF was buffered with tris(hydroxylmethyl)aminomethane (TRIS) to maintain a physiological pH of 7.4. Electrochemical impedance spectroscopy (EIS) and potentiodynamic polarization techniques were used to study the degradation behaviour of the bare metal and the CaP coated samples. A potentiostat and a frequency response analyser (Model VersaSTAT3) driven by VersaStudio, and a typical three-electrode electrochemical cell were used for the electrochemical experiments. The EIS experiments were performed at open circuit potential with an AC amplitude of 5 mV over the frequency range 10^{5} Hz to 10^{-2} Hz. Potentiodynamic polarisation experiments were carried out at a scan rate of 0.5 mV/sec. Prior to the beginning of the electrochemical experiments, the samples were kept immersed in the SBF for one hour to establish a relatively stable potential. Following the polarisation tests, the samples were cleaned with distilled water and examined using SEM to identify the mode of degradation.

RESULTS AND DISCUSSION

Figure 1 shows the conductivity of the coating solution with addition of ethanol. As expected, addition of ethanol decreased the conductivity of the coating solution. The conductivity of the coating solution decreased from 23mS to 16mS when the ethanol content was 10%. Increase in the ethanol content in the coating solution further decreased its conductivity i.e. 30%: 11mS ; 50%: 8mS; and 70%: 5mS.

The current density vs time plots of CaP coating in the different coating solutions are shown in Figure 2. It can be noted that the current density decreased with increase in the addition of ethanol to the coating solution. As a consequence, the thickness of the coating also decreased with increase in ethanol addition (Figure 3). The coating thickness decreased from 12μm to 6μm when the ethanol content was 30%. Increase in the ethanol content to 70% decreased the coating thickness to 2.5μm.

In order to confirm that the hydrogen evolution also decreased with increase in the ethanol addition to the coating solution, cathodic polarisation experiment was carried out on the bare metal in distilled water and ethanol-distilled water mixtures. The cathodic polarisation curves showed that the cathodic current density decreased when the ethanol was added (Figure 4). The decrease in the current density was significantly high when the ethanol content reached 70%. This behaviour clearly indicates that the hydrogen evolution reduced with ethanol addition to the coating solution, since hydrogen evolution reaction is the predominant cathodic reaction for magnesium and its alloys.

The Nyquist plots of the bare metal and the CaP coated alloy in SBF are shown in Figure 5. The bare metal exhibited a high frequency capacitive loop (corresponds to charge transfer resistance) as well as a second mid frequency capacitive loop (corresponds to relaxation of mass transport through the corrosion product layer),[20,21] which suggest that the bare metal was only partially protected in SBF. The polarisation resistance calculated from the capacitive loops was 700 $\Omega.cm^2$. At a low frequency range, the bare metal revealed an inductive loop which suggests that the alloy is prone to pitting corrosion.[22,23] In contrast, the CaP coated alloy in aqueous coating solution showed only one capacitive loop. The polarisation resistance of the coated alloy was

more than an order of magnitude higher than that of the bare metal. The coated alloy exhibited a polarisation resistance of 7.8 x 10^3 $\Omega.cm^2$. A small addition of ethanol (10%) to the coating solution produced a coating (1E) which performed better than the aqueous coating i.e., the polarisation resistance of the 1E coating was 1.2 x 10^4 $\Omega.cm^2$. The polarisation resistance further increased to 1.5 x 10^4 $\Omega.cm^2$ when 30% of ethanol was added to the coating solution. However, when the addition of ethanol to the coating solution was increased to 50%, the polarisation resistance decreased to 1.2 x 10^4 $\Omega.cm^2$. Further increase in the amount of ethanol (70%) decreased the polarisation resistance drastically i.e. 7E coating showed a polarisation resistance of only 2.8 x 10^2 $\Omega.cm^2$.

The polarisation curves of the bare metal and the CaP coated alloy in SBF are shown in Fig 6. The corrosion current density (i_{corr}) calculated based on the cathodic curves indicated that the coating enhanced the degradation resistance of the alloy significantly. The bare metal showed a corrosion current density of 60 $\mu A/cm^2$, whereas the coated alloy exhibited a current density of only 6 $\mu A/cm^2$. Similar to the EIS results, when a small content of ethanol was added to the coating solution, the degradation resistance of the resulted coating increased. The 1E and 3E coatings showed a corrosion current density of 4$\mu A/cm^2$ and 2.5$\mu A/cm^2$, respectively. But, further addition of ethanol decreased the degradation resistance i.e., the corrosion current density of the 5E and 7E coatings was 4$\mu A/cm^2$ and 18$\mu A/cm^2$, respectively. A comparison of the corrosion current density of the coatings produced in different coating solutions suggests that the 3E coating performed better than the aqueous coating and also the 1E, 5E and 7E coatings.

In order to see whether the better performance of the 3E coating as compared that of the aqueous coating was due to the chemical structure change, FTIR analysis

was carried out on those coated samples. Both the coatings showed identical peaks, suggesting that the chemical structure of the coatings was similar (Figure 7). The spectrum showed characteristic phosphate peaks at 1122, 1052 and 984 cm^{-1} and calcium hydroxide peaks at 871 and 784 cm^{-1}. The strong peaks at 1122, 1052 and 984 cm^{-1} corresponds to phosphate.[24] XRD analysis confirmed that the coating mainly composed of dicalcium phosphorous dihydrate ($CaHPO_4 \cdot 2H_2O$) as shown in Figure 8.

The SEM micrographs of the coatings produced in aqueous solution and 30% ethanol containing solution are shown in Figure 9. A few large clusters of particles can be seen in the aqueous coating. A higher magnification of the aqueous coating reveals flower-like morphology of the particles. The packing of the particles is not dense; gaps between the particles are evident. However, the 3E coating showed a different morphology. The large clustering observed in the aqueous coating was less apparent in the 3E coating. The coating particles were neatly stacked and as a result the packing was denser for the 3E coating than that of the aqueous coating.

Figure 10 shows the SEM micrographs of post-degraded CaP coated samples. The aqueous coating showed significant corrosion attack suggesting that the SBF has seeped through the gaps between the particles and corroded the bare metal. However, the 3E coating showed lesser attack as compared to the aqueous coating. The denser packing of the 3E coating has significantly restricted the permeation of SBF through the coating and hence resulted in a better performance.

A closer look at the current-time plots of the coating (Figure 2) shows that there is a repetitive pattern in the current density i.e., a sharp increase followed by a slow decrease, during the coating process in aqueous solution. It is suggested that the sharp increase in the current density occurs when hydrogen bubble bursting removes the

already formed coating and exposes the bare metal. In other words, when the bare metal is exposed due to hydrogen bubble bursting, the electrochemical reaction (equation 2) occurs immediately and as a result the current increases sharply, thereafter the current decreases slowly where the coating grows. The repetitive pattern suggests that there was a competition between the CaP deposition and hydrogen bubble bursting during the coating process and hence the coating was not uniform and showed poor performance. However, this repetitive pattern in the current is less prominent in the coating process in ethanol containing solution. The intensity of the current pattern decreased with increase in the addition of ethanol to the coating solution. This indicates that the hydrogen bubble bursting was less intense in the coating process in ethanol containing coating solution. Hence one could expect a denser packing of coating particles in ethanol containing solution as compared to that in aqueous solution. Accordingly, 3E coating exhibited denser packing than that of aqueous coating. However, it should also be noted from Figure 2 that if the ethanol content was very high e.g. 70%, then the current density was too low and as a result the coating thickness was also low. Hence, the performance of 7E coating was inferior to that of aqueous coating.

CONCLUSIONS

The study showed that by reducing the conductivity of the CaP coating solution i.e. by ethanol addition, hydrogen bubble bursting decreased significantly during the coating process and consequently produced denser packing of CaP coating as compared to aqueous coating. In vitro electrochemical experiments and post-degradation analysis suggest that CaP coating produced in 30% ethanol containing solution possessed significantly higher degradation resistance than that of the aqueous coating. Further

increase in ethanol content (e.g. 70%) in the coating solution produced thin coating and as a result exhibited poor degradation resistance.

The author would like thank Ms. Wallipa Ounnapiruk and Mr. Rhys Walter for their technical assistance. The author is also grateful for the financial support from NACE International, USA.

References

1. Witte F, Hort N, Vogt C, Cohen S, Kainer K, Willumeit R, Feyerabend F. Degradable biomaterials based on magnesium corrosion. Current Opinion in Solid State and Mater Sci 2008;12:63-72.
2. Staiger M, Pietak A, Huadmai J, Dias G. Magnesium and its alloys as orthopedic biomaterials: A review. Biomaterials 2006;27:1728-1734.
3. Bobby Kannan M, Raman RKS. In vitro degradation and mechanical integrity of calcium-containing magnesium alloys in modified-simulated body fluid. Biomaterials 2008;29: 2306-2314.
4. Song G. Control of biodegradation of biocompatible magnesium alloys. Corros Sci 2007;49:1696-701.
5. Walter R, Bobby Kannan M. In-vitro degradation behaviour of WE54 magnesium alloy in simulated body fluid. Materials Letters 2011;64:748-50.
6. Witte F, Kaese V, Haferkamp H, Switzer E, Meyer-Lindenberg A, Wirth CJ, et al. In vivo corrosion of four magnesium alloys and the associated bone response. Biomaterials 2005;26:3557–3563.
7. Ghali E, Dietzel W, Kainer KU. General and localized corrosion of magnesium alloys: A critical review. J Mater Eng Perform 2004;13:7-23.
8. Best SM, Porter AE, Thian ES, Juang J. Bioceramics: past, present and for the future. J European Ceramic Society 2008;28:1319-27.
9. Yen SK, Kua MC. The process of electrochemical deposited hydroxyapatite coatings on biomedical titanium at room temperature. Materials Sci Eng C 2002;20:153-60.

10. Liu DM, Yang Q, Troczynski T. Sol-gel hydroxyapatite coating on stainless steel substrates. Biomaterials 2002;23:691-698.

11. Ishikawa K, Miyamoto Y, Nagayama M, Asaoka K. Blast coating method: New method of coating titanium surface with hydroxyapatite at room temperature. J Biomedical Materials Research 1997;38:129-134.

12. Shi, D. Biomaterials and Tissue Eng, Springer-Verlang Berlin Heidelberg, 2004.

13. Hench LL, Splinter RJ, Allen WC, Greenlee TK. Bonding mechanisms at the interface of ceramic prosthetic materials, J Biomed Mater Res 1972;5:117–141.

14. Yang YZ, Kim KH, Joo LO. A review on calcium phosphate coatings produced using a sputtering process – an alternative to plasma spraying, Biomaterials 2005;26:327–337.

15. Song Y, Zhang S, Li J, Zhao C, Zhang X. Electrodeposition of Ca-P coatings on biodegradable Mg alloy: in vitro biomerralization behaviour. Acta Biomaterialia 2010;6: 1736-42.

16. Wang HX, Guan SK, Wang X, Ren CX, Wang LG. In vitro degradation and mechanical integrity of Mg-Zn-Ca alloy coated with Ca-deficient hydroxyapatite by the pulse electrodeposition process. Acta Biomaterialia 2010;6:1743-48.

17. Bobby Kannan M, He Y, Sandham A. Calcium phosphate deposition on magnesium alloy for bioimplant applications. Materials Science Forum 2010;654-656:2196-2199.

18. Redepenning J, Schlessinger T, Burnham S, Lippiello L, Miyano J. Characterization of electrolytically prepared brushite and hydroxyapatite coatings on orthopedic alloys. **J** Biomed Mater Res 1996;30:287–294.

19. Oyane A, Kim H, Furuya T, Kokubo T, Miyazaki T, Nakamura T. Preparation and assessment of revised simulated body fluids. J Biomedical Mater Res A 2003;65:188-95.

20. Pebere N, Riera C, Dabosi F. Investigation of magnesium corrosion in aerated sodium sulphate solution by electrochemical impedance spectroscopy. Electrochim Acta 1990;35:555-61.

21. Baril G, Pebere N. The corrosion of pure magnesium in aerated and deaerated sodium sulphate solutions. Corros Sci 2001;43:471-84.

22. Jin S, Amira S, Ghali E. Electrochemical impedance spectroscopy evaluation of the corrosion behaviour of die cast and tixocast AXJ530 Mg alloy in chloride solution. Adv Eng Mater 2007;9:75-83.

23. Chen J, Wang J, Han E, Dong J, Ke W. AC impedance spectroscopy study of the corrosion behaviour of an AZ91 magnesium alloy in 0.1 M sodium sulphate solution. Electrochim Acta 2007;52:3299-309.

24. Pecheva EV, Pramatarova LD, Maitz MF, Pham MT, Kodyuiriin AV. Kinetics of hydroxyapatite deposition on solid substrates modified by sequential implantation of Ca and P ions, Part I. FTIR and Raman spectroscopy study. Applied Surface Science 2004;235:176-181.

TABLES

TABLE I

Chemical composition of AZ91 alloy

Al	Zn	Mn	Si	Fe	Mg
9.18	0.78	0.20	0.01	0.002	Bal.

TABLE II

Composition of simulated body fluid [19]

Reagent	Amount
NaCl (g/L)	8.036
$NaHCO_3$ (g/L)	0.352
KCl (g/L)	0.225
$K_2HPO_4 \cdot 3H_2O$ (g/L)	0.230
$MgCl_2 \cdot 6H_2O$ (g/L)	0.311
1.0 M HCl (mL/L)	40
$CaCl_2$ (g/L)	0.293
Na_2SO_4 (g/L)	0.072
TRIS buffer[a] (g/L)	6.063

[a] TRIS buffer = tris(hydroxylmethyl)aminomethane

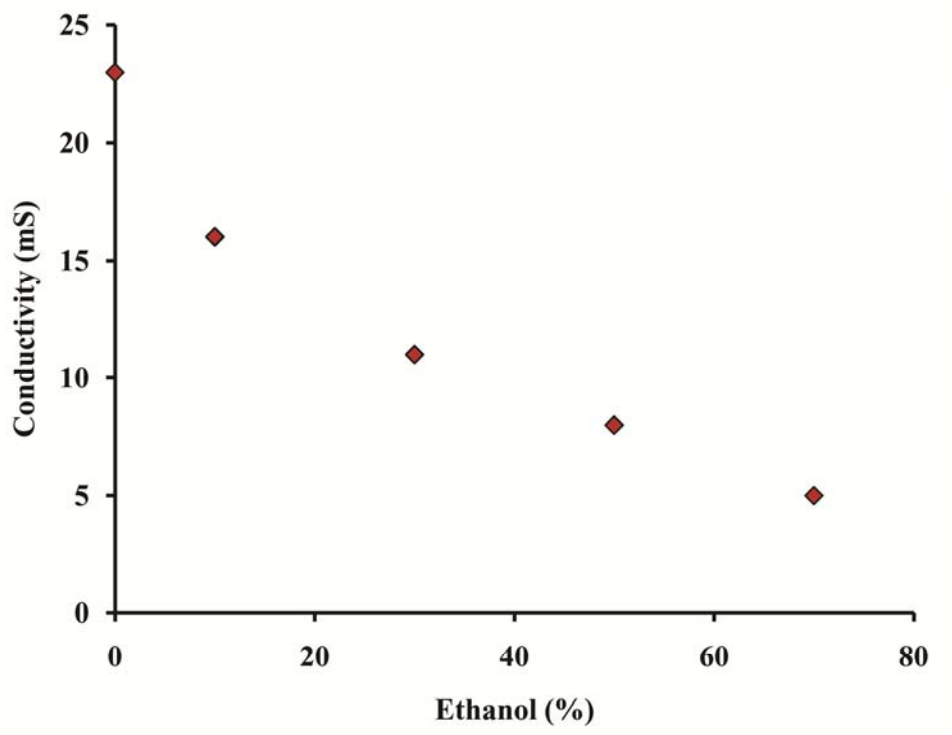

Figure 1. Conductivity of the coating solution with addition of ethanol.

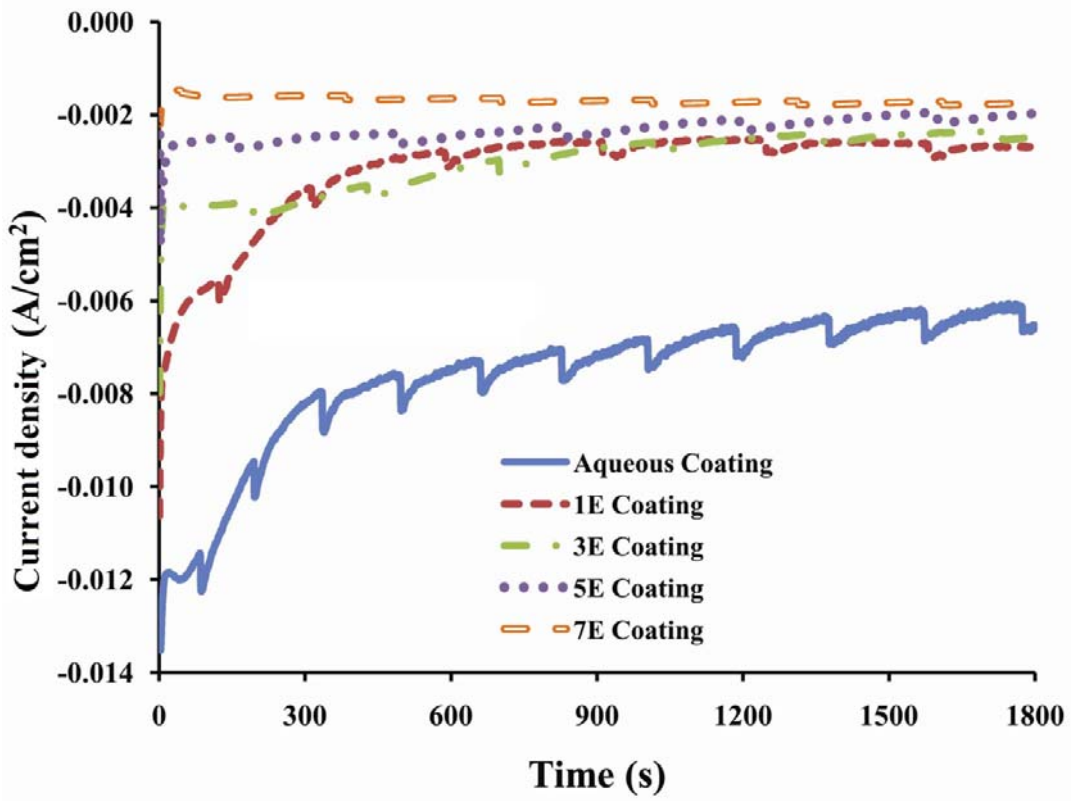

Figure 2. Current density vs time plots of AZ91 magnesium alloy coated at -3V in different coating solutions.

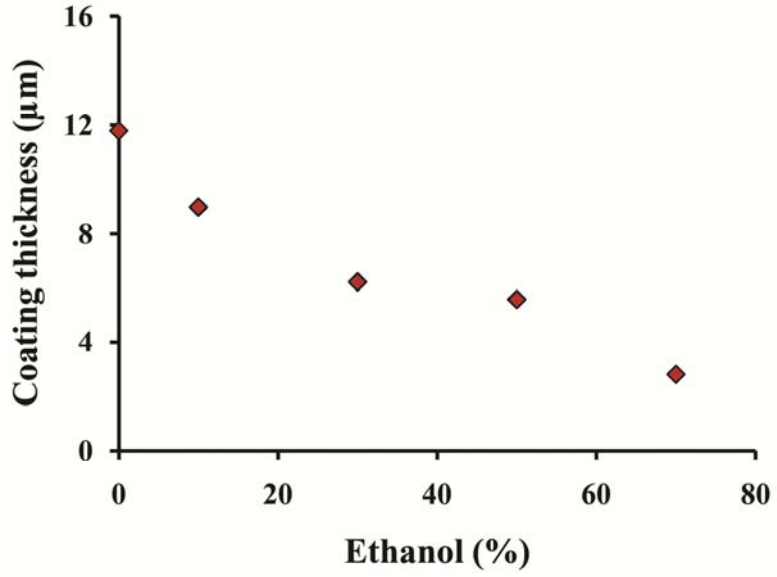

Figure 3. Coating thickness on AZ91 magnesium alloy with addition of ethanol to the coating solution.

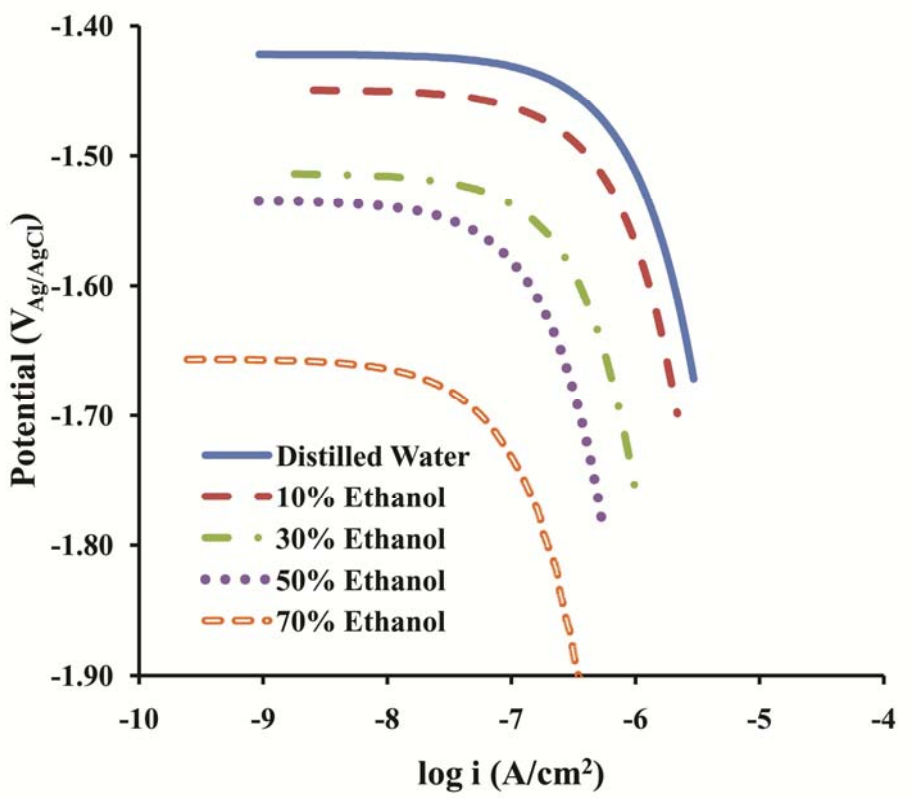

Figure 4. Cathodic polarization curves of AZ91 magnesium alloy in distilled water (DW) and in DW/Ethanol mixtures.

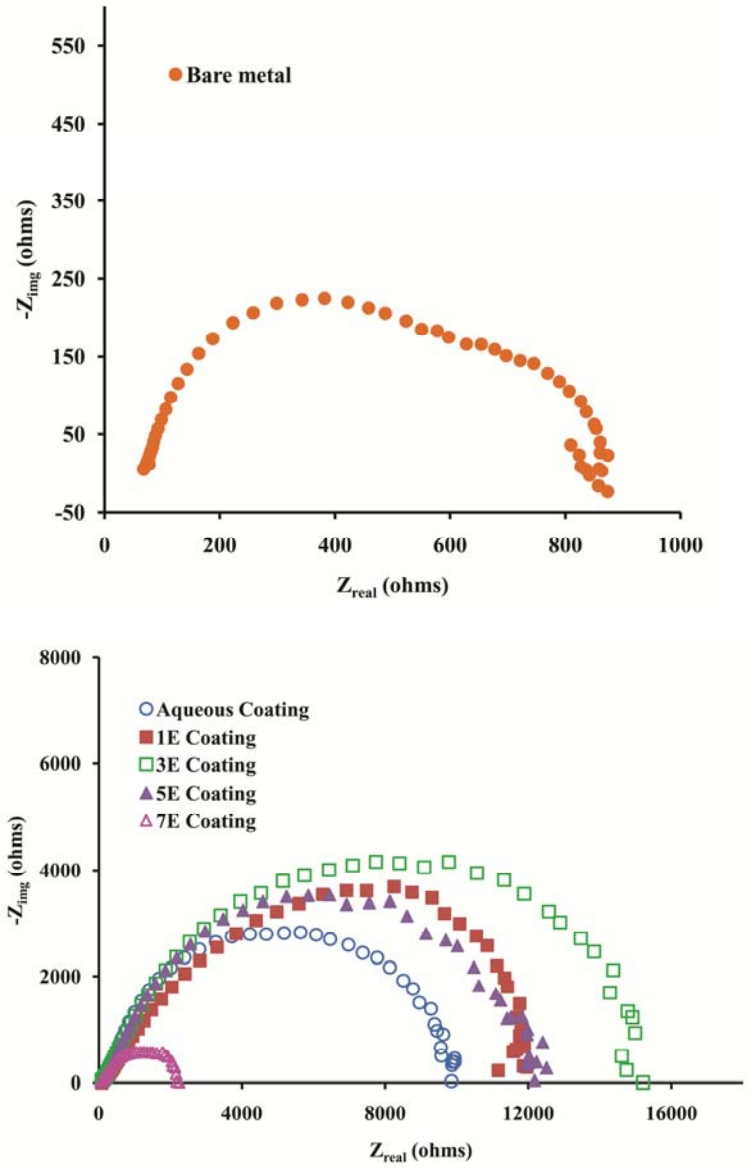

Figure 5. Nyquist plots of (a) bare metal and (b) CaP coated samples (in different coating solutions) in simulated body fluid at 37°C.

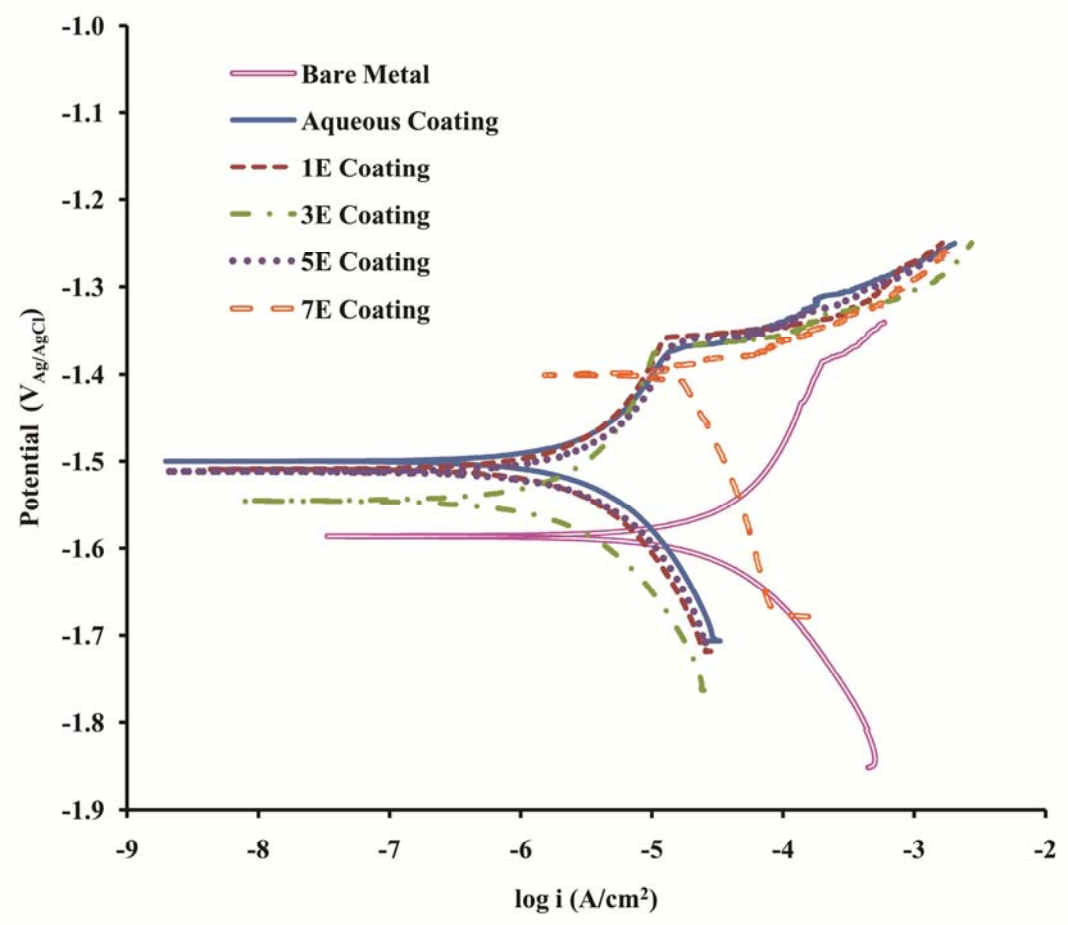

Figure 6. Potentiodynamic polarisation curves of bare metal and CaP coated samples (in different coating solutions) in simulated body fluid at 37°C

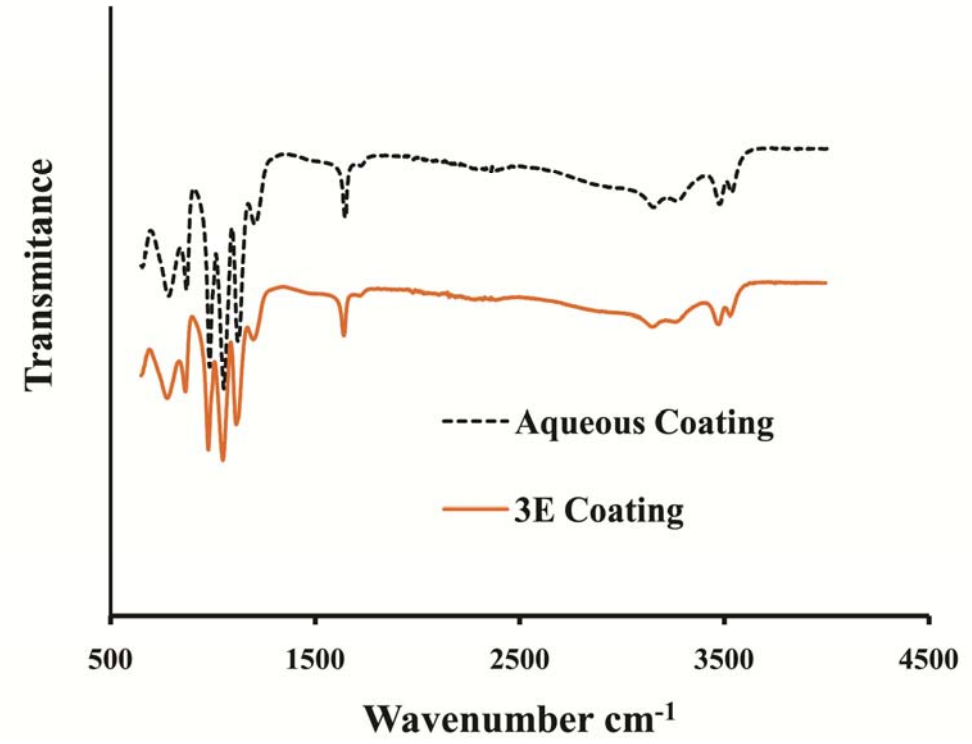

Figure 7. FTIR spectra of aqueous solution and 30% ethanol containing solution coatings.

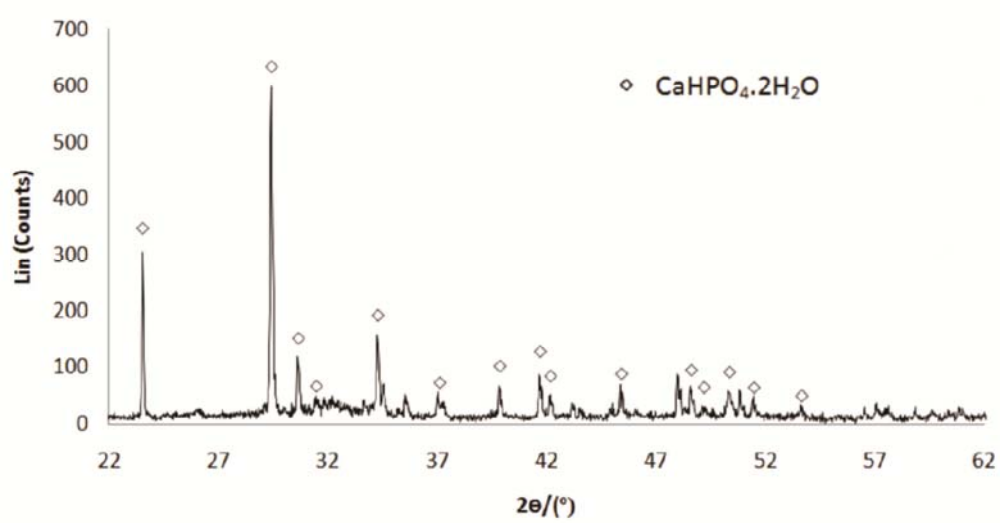

Figure 8. XRD spectra of aqueous solution coating.

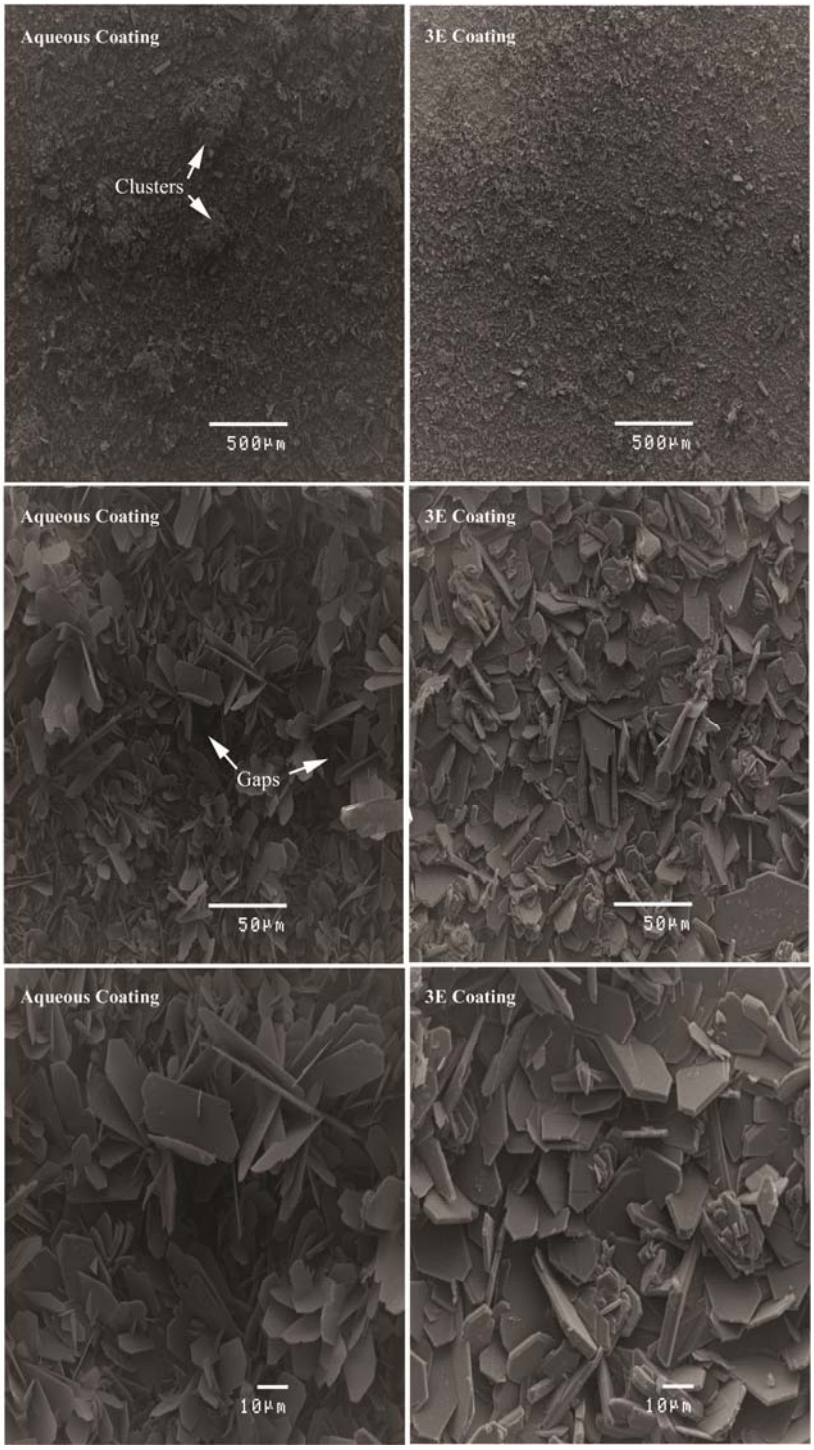

Figure 9. SEM micrographs of aqueous solution and 30% ethanol containing solution coatings.

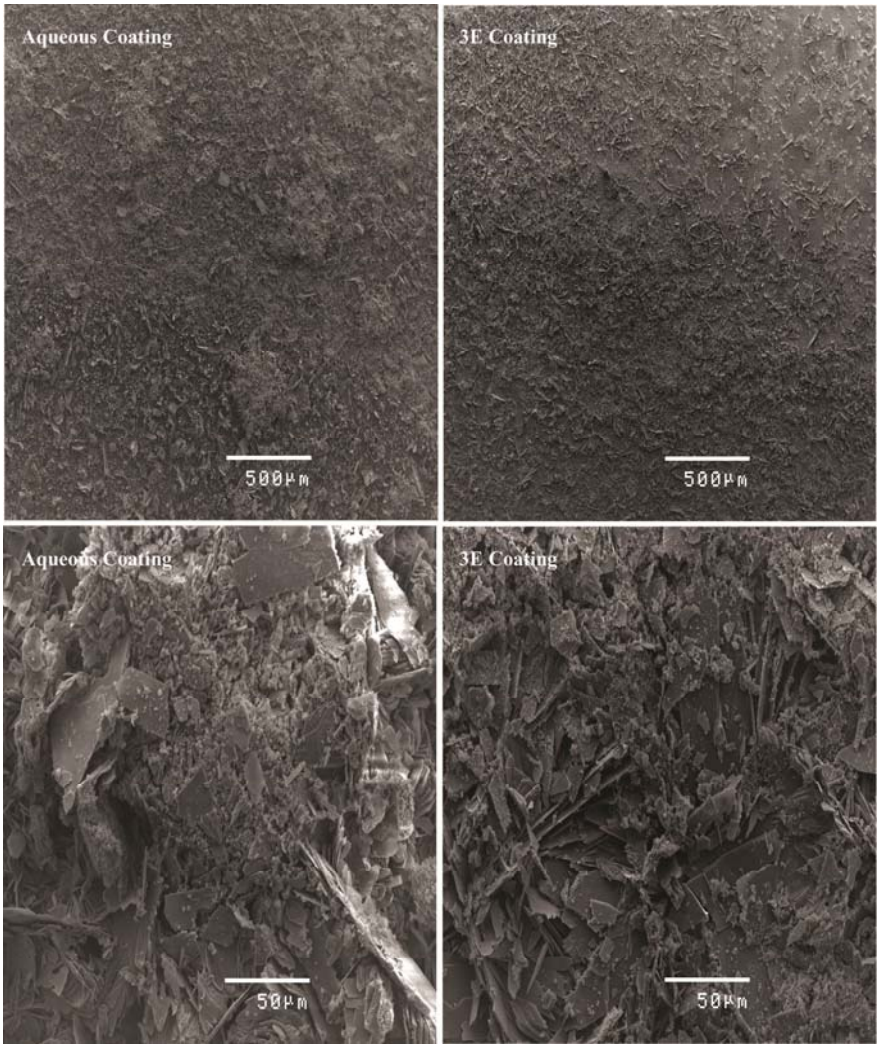

Figure 10. SEM micrographs of aqueous solution and 30% ethanol containing solution coatings after degradation in simulated body fluid at 37°C.